INTERNATIONAL DESIGN CONFERENCE – DESIGN 2022
https://doi.org/10.1017/pds.2022.141

Data-Driven Design Support for Additively Manufactured Heating Elements

K. Hilbig✉, M. Nowka, J. Redeker, H. Watschke, V. Friesen, A. Duden and T. Vietor

Technische Universität Braunschweig, Germany

✉ k.hilbig@tu-braunschweig.de

Abstract

Additive Manufacturing (AM) enables innovative product designs. One promising research field is AM of integrated electrically structures, e.g. heating panels using Joule effect. A mayor challenge in designing heating panels using AM is the dependency of its resultant resistivity from material, process and geometry parameters. The goal-oriented design of heating panels with individual surface temperatures the interactions between these parameters need to be understand. Therefore, a data-driven design approach is developed that facilitates a design of heating panels with specific properties.

Keywords: data-driven design, design support system, additive manufacturing, electrically conductive polymers, heat-generating structures

1. Introduction

Additive manufacturing (AM) provides enhanced freedom in product or part design. One of these new design possibilities is multi-material design that allows a combination of multiple materials in one part without additional joining or assembly processes. Due to its easy handling and a great variety of available materials in material extrusion(MEX) has been established for multi-material, especially for the integration of additional functions like electrical conductivity, e.g., for sensing elements (Leigh et al., 2012) or integrated heating panels using the Joule effect (Dul et al., 2018; Watschke et al., 2019). While AM of sensors has already been investigated in many studies, there has been only isolated research in the area of heat-generating structures. However, additively manufactured heating panels with individualized shapes and properties could provide a vast potential. AM enables local control of the heat distribution by an adjustment of electrical resistivity due to a variation of part orientation and geometry (e.g., lattice structures) (Watschke 2019), process parameters (Watschke et al., 2019; Hilbig et al., 2020), or material distribution (Dul et al., 2018; Zhuang et al., 2017). Thus, it is possible to adjust the surface temperature of heating panels individually.

To fully utilize this potential new design methods or tools are necessary for describing the interactions between process-specific influencing factors and the part's resultant electrical resistivity. Therefore, in this contribution a data-driven design approach is developed, that enables designing heating panels with customizable homogeneous surface temperatures.

2. State of the art

This section describes the main leverages of MEX for electrical resistivity and heat distribution. Furthermore, it provides an introduction to data-driven strategies in process and design domains in the context of AM.

2.1. Influences on additively manufactured electrically conductive structures

Additive manufacturing of electrically conductive structures enables adjustment of part's resultant electrical resistance and surface temperature by both geometry, process parameters as well as the applied voltage. Thus, the resistivity is not only determined by the selected material, but also by the manufacturing process. Influencing factors on the resistivity related to the process are: build orientation (Dul et al., 2018; Zhang et al, 2017), layer height (Hampel et al., 2017; Zhang et al., 2017), raster angle orientation (Watschke et al., 2019; Hilbig et al., 2020), extrusion width (Zhang et al., 2017), flow rate (Zhang et al., 2017; Watschke et al.; 2019; Hilbig et al., 2020), extrusion temperature (Hampel et al., 2017; Watschke et al., 2019; Hilbig et al., 2020), and cooling (Hampel et al., 2017). The raster angle has the biggest effect on resistivity. Therefore, the adjustment of this parameter has the main leverage of the surface temperature by the electrical resistivity of the heating panel (Watschke et al., 2019; Hilbig et al., 2020; Tirado-Garcia et al., 2021). Watschke, (2019) and Kim et al., 2020 investigated the head distribution by alternatives geometries like honeycomb and lattice structures.

2.2. Machine learning approaches in design for additive manufacturing

The design freedom provided by AM to adjust mechanical and electrical part properties by geometry and process parameters leads to an increased dimensionality of the design space. Trade-offs between objectives and constraints imposed by the manufacturing process make it even more challenging to find optial and feasible design solutions. Therefore, new approaches are required to effectively screen the multi-dimensional design space to exploit the full potential for product design. In general, a classification can be made between data-driven and model-based design strategies to support design exploration and exploitation for AM (Zhang et al., 2021). Design exploration is dedicated to quickly identifying all design alternatives that satisfy a range of design objectives and are related to the early design stages. In comparison, design exploitation has the target to search for a design with maximum performance for defined criteria (Xiong et al., 2019). Model-based approaches utilize a priori knowledge of the underlying physical knowledge of the process. These principles are then subsequently used to build a process model for simulation, which is then verified and validated (Yin et al., 2014). On the other hand, data-driven strategies are the approach of integrating, analysing, and processing collected data from multiple sources (e.g., experimental, simulation and sales data) to get insights into the underlying problem (An et al., 2015). In general, more cost-effective and faster explorations and predictions are possible through data-driven techniques (Zhang et al., 2021; cf. Roy and Wodo, 2020). Data-driven design approaches for AM are primary based on supervised (e.g., Bayesian methods (Bessa et al., 2019) or artificial neural networks) machine learning methods. In the context of data-driven design strategies for MEX, approaches address, for example, dimensional accuracy (Wang et al., 2018), determining printable bridge lengths (Jian et al., 2019) or predicting thermal field during the manufacturing process. A detailed overview of data-driven strategies in AM can be found in the article by Zhang et al. (2021).

3. Acquisition of data for the design exploration approach

The following section presents the design of experiments, the set-up of the additive manufacturing process and the verification procedure for the determination of the resistivity and the voltage as well as process parameter-dependent heat distribution.

3.1. Test specimens configuration for planar heating structures

A D-optimal design space with a quadratic trial function is used for the design of experiment. In favour of the selection of the input factor the studies of Watschke et al., 2019 and Dul et al., 2018a were taken into consideration. The determination of the input factor was defined as categorical levels of the printing temperature of 210°C – 250°C with a step size of 10°C. Raster angle, see examples in Figure 1, of 0° – 90° with a step size of 10°, including the 45° orientation to the current flow. An orientation of 0° is parallel, whereas 90° is orthogonal to the current flow.

https://doi.org/10.1017/pds.2022.141 Published online by Cambridge University Press

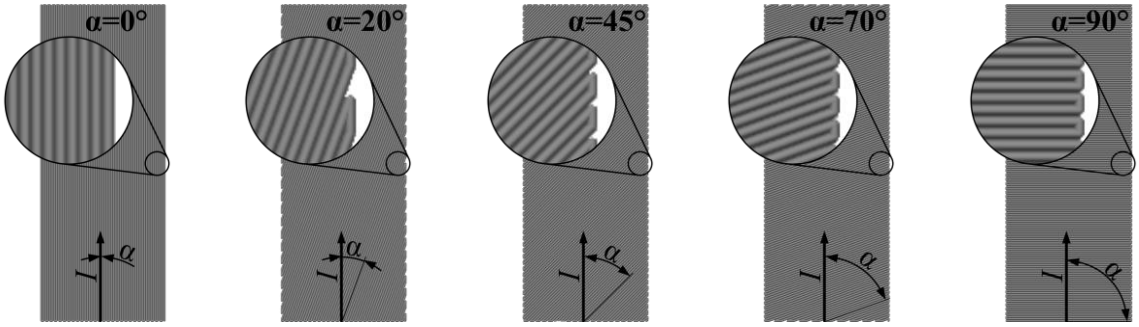

Figure 1. Examples of investigated infill orientations by the raster angle (α) in relation of the current flow during sourcing

The design space results in a total number of 60 different process parameter sets with three specimens per set (180 in total). The dimensions of the test specimens, see Figure 2, were defined by microscope slides on which the specimens were manufactured. To investigate the optimal electrical contacting method of the specimens three variants were considered and evaluated, see Figure 2.

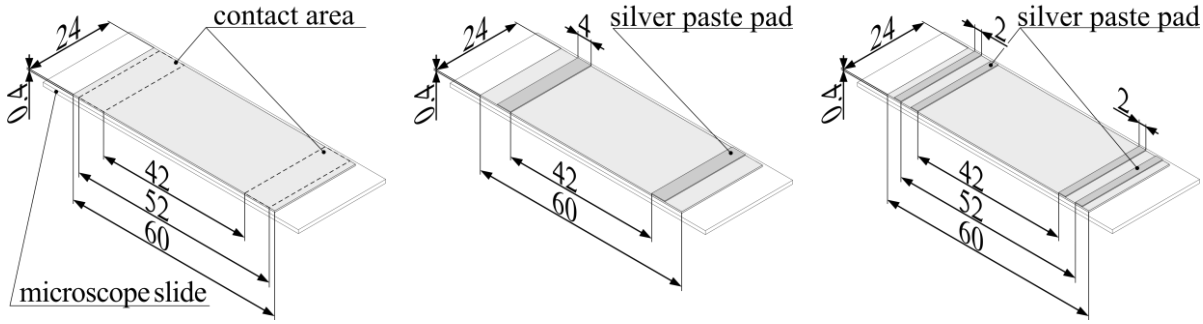

a) Contacting without contact resistance reducing techniques

b) Contacting with two silverpaste pads for combined sourcing and sensing

c) Contacting with two silverpaste pads for sourcing and two for sensing

Figure 2. Isometric view and dimensions of the test specimens and contacting variants

In this research, the material BlackMagic3d PLA-Conductive (Graphene Laboratories, 2020) was used. To prevent hydration of the material a preconditioning process step of drying the filament was carried out at a temperature of 60°C for 24 hours. The selection of the preconditioning temperature was based on the matrix polymer of the filament. In order to avoid water absorption of the filament during production, the manufacturing process was carried out immediately after drying in standard atmosphere at room temperature at 22±2°C and relative humidity of 60±5%. The test specimens were manufactured with a Toolchanger® (E3D) using a Hemera® (E3D) direct extruder with a brass nozzle with diameter of 0.4mm. Other process parameters such as the printing bed temperature (60°C) and a manufacturing speed (40mm/s) were kept constant throughout the manufacturing process of all specimens. Due to the height of the specimen of 0.4mm, a layer height of 0.2mm was chosen, both of the layers are fabricated in the same raster angle, e.g. +45° / +45°. In preparatory tests, the material-dependent flow was set with the aim of producing a true-to-scale.

3.2. Introduction of the measurement set-up and the applied methods

In order to characterize the electrical behaviour of the specimens, the resistivity was investigated. Relating to the resistance, resistivity is a geometry-independent property and is equal to the inverse conductivity of a material. The resistivity is defined in Equation 1 as:

$$\rho = R \cdot \frac{A}{L} = \frac{U}{I} \cdot \frac{b \cdot h}{l} \left[\frac{\Omega m^2}{m}\right] \tag{1}$$

https://doi.org/10.1017/pds.2022.141 Published online by Cambridge University Press

The geometrical influences of the used specimen remain constant. The cross-section (A) of the specimen, see Figure 2, is defined by the product of width (b) and height (h). The distance between the contacted measuring pads (l) also remains constant due to the test rig and the connection variants. Therefore, the only varying factor is the resistance (R), which can be determined with the electrical parameters current (I) and voltage (U). The current and voltage are measured with a calibrated Keithley 2461 Sourcemeter.
A test rig (see Figure 3a) is used to ensure constant conditions for the hook-up of the specimen to the sourcemeter and for the positioning of the specimen in the focal point of the thermal imaging camera. The sample is placed in the test rig and then the lever is used to clamp the specimen between the four jaws. Each jaw is equipped with 3x8 spring-loaded contacts. These contacts exert a force of approximately 0.6N per contact against the sample during measurement. Figure 3b shows an example of the wiring set-up for a 4-wire measurement.

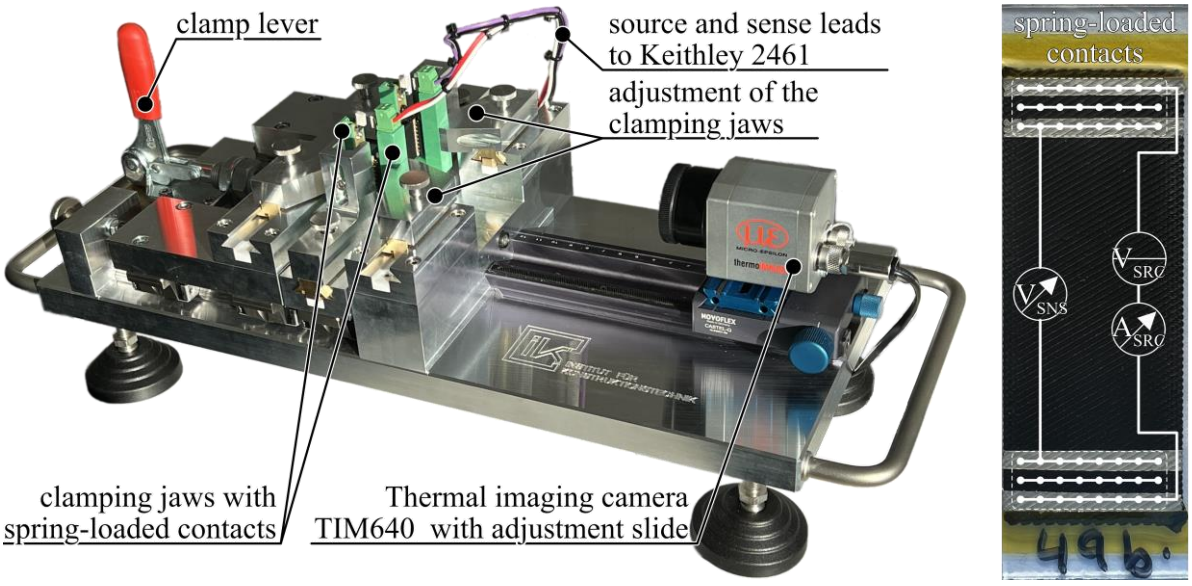

a) Test rig for hook-up of the sourcemeter and for precise alignment in front of the thermal imaging camera; b) Specimen wiring for 4-wire measurement

Figure 3. Overview of test rig and contact set-up of the specimens for 4-wire measurement

Depending on the wiring of the spring-loaded contact pin rows 2- as well as 4-wire measurements can be carried out with the test rig. In a 4-wire measurement configuration, see Figure 4b,d, the two outer rows of contact pins are sourcing while the two inner rows are sensing the voltage drop over the length (l). By measuring the voltage drop over the length of the specimen, the contact resistance can be largely eliminated from the measurement. Whereas measuring the resistivity by the 2-wire measurement, see Figure 4a,c, the applied voltage is measured in the source meter and the current is sourced into the specimen via the two inner rows of spring-loaded-contacts. This method ensures that the sample length over which the measured voltage drop occurs is identical to the 4-wire measurement, but the contact resistance can not be eliminated by sensing the voltage in the sourcemeter. The contact resistance can be reduced by applying an electrical contract agent, e.g. silver paste EMS12640 (Figure 4c,d).
The temperature distribution can be recorded with a resolution of 640x480px using the TIM 640 thermal imaging camera and 33° optics from Micro Epsilon. The camera is positioned at a distance of $180mm$, achieving a resolution of $170\mu m/px$. By clamping the specimens between the two jaws, the specimens were positioned precisely in the focal point of the thermal imaging camera.

https://doi.org/10.1017/pds.2022.141 Published online by Cambridge University Press

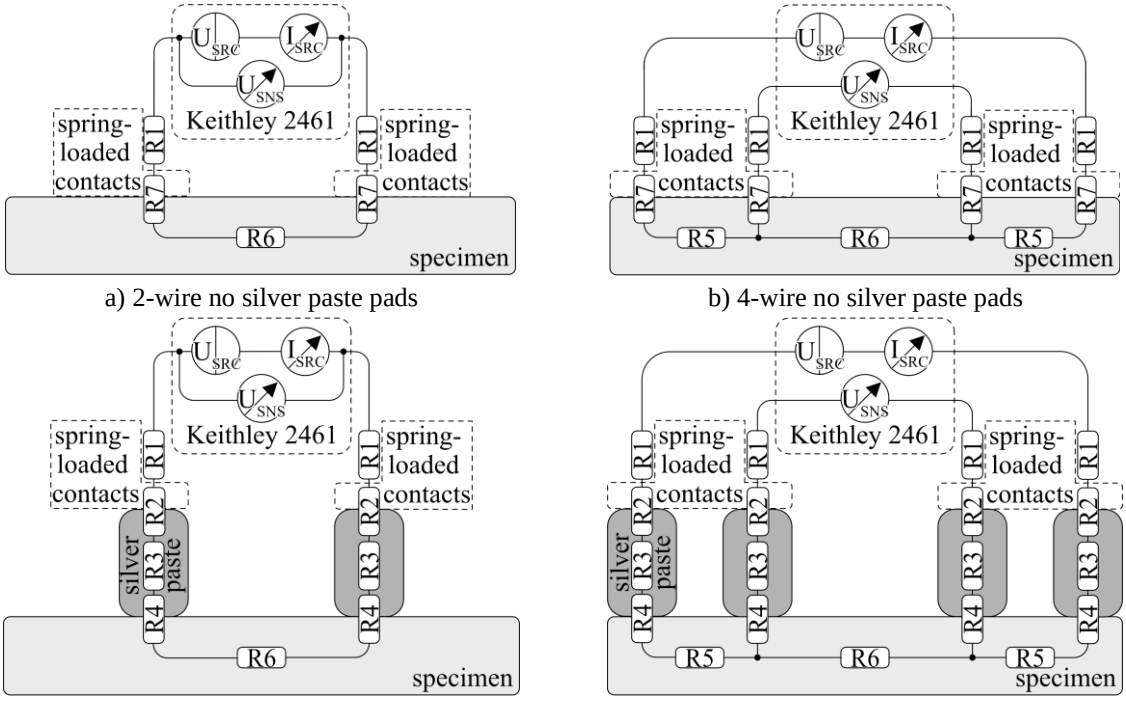

a) 2-wire no silver paste pads

b) 4-wire no silver paste pads

c) 2-wire with silver paste pads

d) 4-wire with silver paste pads

R1: test lead resistance; R2: contact resistance between spring-loaded contacts an silver paste pads; R3: internal resistance of silver paste pad; R4: contact resistance between specimen an silver paste; R5: internal resistance of specimen between source and sense location; R6: internal resistance of specimen between low- and high-side sense location; R7: contact resistance between spring-loaded contacts and specimen

Figure 4. Schematic overview of contacting variants

3.3. Electric connection of additively manufactured structures

To minimize the contact resistance of the samples an investigation of the electric bonding method was performed. Therefore, the combination possibilities can be categorized into three options:

- coating of contact area: none (a1) or with an electrical bonding agent (a2)
- number of contact pads: combined pads (b1) or separated pads for sensing and sourcing (b2)
- measurement method: 2-wire (c1) or 4-wire measuring (c2)

In order to minimize the contact resistance (a2) the bonding agent silver paste EMS 12640 is applied at the specified location based on the two variants as depicted in Figure 2a,b.

To identify the ideal combination of the three options, specimens were produced with the same process parameters. Each of the contacting methods was applied to five specimens and the resistivity was measured. For a comparison, a representative specimen of each combination is shown, see Figure 5.

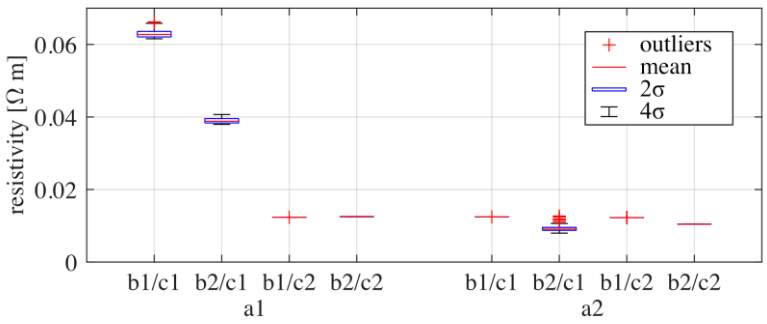

a1) without silver paste pads; a2) with silver paste pads; b1) combined silver paste pad for souring and sensing; b2) separated silver paste pad for souring and sensing; c1) 2-wire measurement; c2) 4-wire measurement

Figure 5. Comparison of the resistivity by the contacting variants using a representative specimen for each variant

https://doi.org/10.1017/pds.2022.141 Published online by Cambridge University Press

The main difference of the contact method is whether the contact surface is coated with or without silver paste, comparison of group a1 and group a2. The group with the silver paste has a lower contact resistance across all subgroups. As assumed in the group without silver paste (a1) the 4-wire measurement method shows that most of the contact resistance is eliminated by this measurement method. In comparison of the main groups (a1 vs. a2) the 4- wire measuring has the minimal contact resistance with minimal scattering of the data points. Across all the contacting methods, the variant with silver paste (group a2), with a separated silver paste pad for sourcing and sensing (group b2) and the 4-wire measuring method (group c2) caused the lowest contact resistance for the specimens. Thus, for all further measurements, contacting will be made with separate pads for sourcing and sensing with silver paste. Where possible, 4-wire measurement is preferred.

3.4. Measurement of the temperature-dependent resistivity due to self-heating

First of all, the resistivity of all specimens was measured at 22°C ± 2°C with a 4-wire measurement, see Figure 3b. The current is sourced through the two outer contact rows, which is regulated by an applied voltage of $1V$ between the inner contact rows. The resistivity is calculated from the voltage, the current and the geometry parameters between the two sense silver paste pads.
For the application in heating panels, the temperature-dependent resistivity due to self-heating is measured. For this purpose, the specimens are supplied with higher voltages, which allows only 2-wire measurements due to the restriction of the sourcemeter. The surface temperature is recorded with the thermal imaging camera at a distance of 180mm. The schematic set-up is shown in Figure 6.

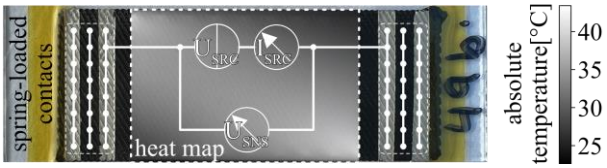

Figure 6. Schematic circuit diagram of the specimen wiring and exemplary superimposition of the resulting heat distribution at 11V of a specimen with α=30° at 22°C ambient temperature

At the start of the measurement, a voltage of 10V is applied on the specimens. The electrical power is converted into heat in the specimen and heats it, via the Joule's effect. This leads to a measurable change in resistivity. Therefore, the resistivity is continuously calculated from the measurement data and the time derivative $d\rho/dt$ is formed. An empirical threshold of $|d\rho/dt| \leq 2.2 \cdot 10^{-6}\Omega\,(\mathrm{m\ s})^{-1}$ is chosen as the threshold criteria for the resistivity to be considered sufficiently static. As soon as the resistivity falls below this threshold, it is measured 100 times and stored. Then a thermographic image associated with the resistivity is taken. The highest surface temperature is determined from the thermal image. If the temperature is below the polymer's heat deflection temperature of 60°C, the voltage is increased by 1V and maintained until the resistivity can be considered constant at the newly set voltage according to the threshold criteria. This process is repeated until the heat deflection temperature is exceeded.

4. Development of a data-driven design exploration approach for heating panels

The following chapter presents the data-based approach that enables efficient exploration of the design space for heating structures based on the previous experiments. Thereby, the scope is on supporting the process parameter selection of additively manufactured heating panels given a target temperature and a nominal voltage as input while maintaining the constraints of homogeneous heat distribution on the specimen's surface. First, the basic approach for the design support of the heating panels is presented. Based on this, the implementation, followed by the evaluation of the method, is described.

4.1. Approach for data-driven design space exploration for heating panels

The approach is divided into two core modules: regression model-based prediction of process parameter sets, followed by their classification into feasible and infeasible temperature distributions. These two modules are processed sequentially. Figure 7 visualizes the structure of the method to be implemented.

https://doi.org/10.1017/pds.2022.141 Published online by Cambridge University Press

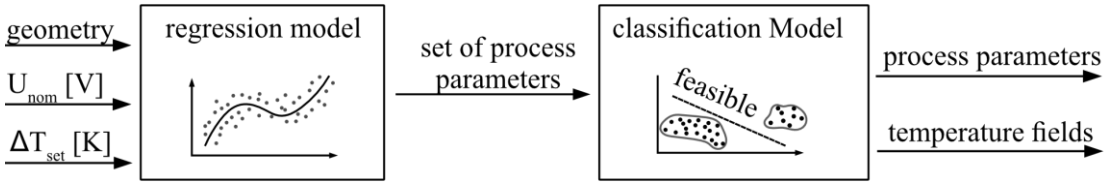

Figure 7. General approach for data-driven design exploration for heating panels

A regression model is trained with the acquired data. Initially, the measurements taken in Section 3.4 will serve as the primary training data. The model will thus be able to predict the process parameter sets that lead to the aspired electrical properties and thermal distribution of the heating panels surface based on the user specifications of nominal voltage U_{nom}, target temperature difference ΔT_{set} and geometry of the heating panels. The output of the regression should represent design recommendations that lead to the target temperature with low deviation. The aim is thus to extract parameter sets that are as robust as possible with respect to uncertainties in the manufacturing process and in the regression model. These are in this case raster angle and nozzle temperature (see Section 3.2). Therefore, the model represents two levers for adjusting the part properties that have a significant influence on the resistivity and thus on the heat distribution (cf. Watschke et al., 2019; Hilbig et al., 2020).

In the context of this work, the objective for the design of the heating panel is a homogeneous temperature distribution on the surface. The distribution is primarily influenced by the geometry, raster angles and the electrical contacting of the panels (Watschke et al., 2019). To separate feasible and infeasible designs, a classification model is trained based on the previous generated thermal images. Therefore, the captured images have to be labelled as feasible or infeasible manually or by a suitable clustering algorithm. Based on the predicted process parameter sets and geometric boundary conditions, the trained classifier should be able to specify the probable temperature distribution. In addition, designs with inhomogeneous heat distributions should be eliminated. The geometric parameters are constant in this work. In the future, it should be possible to predict the heat distribution based on measurements and simulations of varying and complex surfaces of heating panels, e.g. by encoding the geometry using 3D-shape descriptors (cf. Reuter et al., 2006).

4.2. Implementation of the approach for data-driven design space exploration

The implementation of the method for data-driven design space exploration for heating panels is done in version 3.8 of Python. In addition, the machine learning libraries Scikit-learn (v. 1.0.1) and Keras (v. 2.7.0) were used to realize the regression and classification tasks. For the regression model to predict appropriate process parameter sets, a Gaussian process regression (GPR) is utilized. In GPR kernel functions are used to define a prior distribution over the target functions and the input data to define a likelihood function. Based on Bayes theorem, a posterior distribution is defined over the target functions, the mean of which is used for prediction. The model's advantage is thus, that the variance in the input data due to uncertainties in heating panel manufacturing, measurements, and the regression model can be well captured. Consequently, the uncertainty of the predictions of a parameter set on the target temperature can be easily included in the design decision process.

Instead of a multi-target regression approach, an inverse parameter identification strategy is followed. Thereby, a sampling of potential process parameter combinations is initially generated. The samples are passed to the trained regression model to predict temperature and associated standard deviation of the output. If the predicted temperature is within the defined tolerance range, the combination is labelled as a potential design candidate for later passing to the classification algorithm. Besides, the brute force approach an optimization algorithm can be utilized to determine an optimal parameter set.

For training and evaluating the performance of the GPR model, the data set consisting of 1727 samples is split into a training and test data set (ratio of 1/5). The used covariance functions is a composition of squared exponential and White Kernel with optimized hyperparameters estimated by L-BFGS-B algorithm. The quality of the trained model is measured with the coefficient of determination $R^2 = 0.94$. Whereas a R^2 above 90% promises sufficient prediction quality of the model. Furthermore, the residual distribution points out that the error is normally distributed around zero, which generally indicates a well-fitted model.

https://doi.org/10.1017/pds.2022.141 Published online by Cambridge University Press

For the classification task of the predicted process parameter sets concerning their resulting heat distribution, the workflow shown in Figure 8, is implemented based on the collected thermal images.

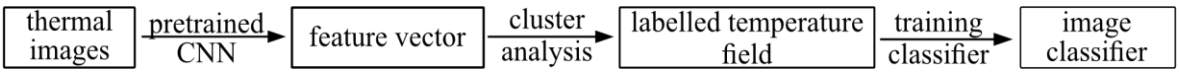

Figure 8. Flowchart for training the classifier for the estimation of feasible heat distributions

To be able to train a classification algorithm, it is first necessary to group the collected data into feasible and infeasible heat distributions and thus label them on this basis. For this purpose, unique feature vectors are first extracted from the samples using a transfer learning strategy. In this work, the Deep Convolutional Neural Network (CNN) VGG16 for image classification tasks (Simonyan et al., 2014) implemented in Keras is used. The pre-trained network is treated as an arbitrary feature extractor, allowing the input image to propagate forward, stopping at a pre-specified layer and taking the outputs as the features for the further clustering task. Here, the final softmax layer, which is responsible for the final classification, has been removed from the VGG16 architecture. Therefore, the new final output of the network and thus each unique feature vector has 4096 components characterising the thermal image.

Before applying the density-based clustering algorithm DBSCAN on the extracted feature vectors to identify patterns based on the visual similarities of the heat distributions, a dimensionality reduction is performed. By applying principal component analysis (PCA) the feature vectors are reduced to 200 principal components whereas 95.54% of the variance of the original feature space can be kept. Next, the feature vectors are fed to DBSCAN. Thereby, the optimum value for the search radius ε was determined based on the work of Rahma and Sitanggang, (2016) and the minimum samples default value is kept. The applied metric is the Euclidean distance. Figure 9 shows the extracted 8 main clusters.

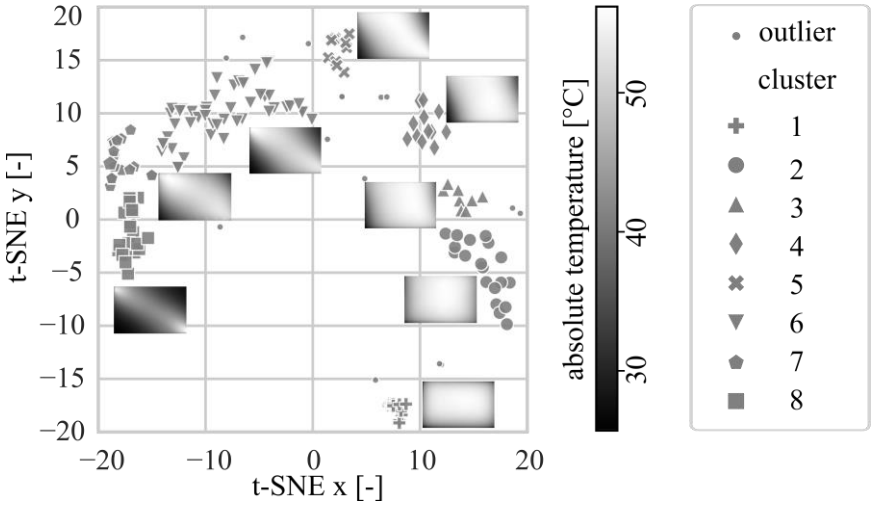

Figure 9. DBSCAN results based on reduced feature vectors of thermal images

Thereby, for visualization purposes, the feature vectors are embedded into 2D-space using t-SNE algorithm and only the data points corresponding to the last thermal images captured before reaching the threshold criteria (see Section 3.4) are depicted. For training the classifier, all images corresponding to clusters 1 (raster angle 90°) and 2 (raster angle 0°) are labelled as feasible, since they show the most homogeneous temperature distribution. Concerning the nozzle temperature, no significant influence on the cluster formation and thus the heat distribution can be identified. The voltage has no effect on the homogeneity. This observation is consistent with the previous studies.

Finally, the k-nearest neighbours (kNN) classification algorithm is trained based on the labelled data set. An accuracy score of 96.3% is achieved with the default settings of the Scikit-learn implementation of kNN. Whereas, the accuracy score is defined as the quotient between the number of correct predictions and the total number of predictions. Thus, a classification of the predicted process parameters into feasible and infeasible solutions can be performed. Furthermore, temperature images of the nearest neighbours can be returned to evaluate the predicted temperature distribution in detail.

https://doi.org/10.1017/pds.2022.141 Published online by Cambridge University Press

4.3. Design support tool for additively manufactured heating panels

The design space exploration method presented in the previous section was integrated into a dashboard using the Python library Panel (v. 0.12.4) that will be presented in detail in further publications. In addition to the recommendation system for robust process parameters, the support tool provides additional functionalities in the context of data pre-processing, e.g., for visual outlier detection, correlation and sensitivity analysis, and the initial comparison of various regression model approaches (e.g., random forest and gradient boosted regressor) to evaluate their performance in the context of the present data. In the dashboard, the user is able to enter the desired temperature difference of the heating panel, a tolerance range as well as the nominal voltage. The tool returns a list of suitable process parameters that have been labelled as feasible or infeasible (homogeneous heat distribution) using the classifier. Additionally, the predicted standard deviation of the temperature is returned. By selecting a parameter set, a thermal image is additionally shown based on the classifications.

5. Conclusion

In this research, AM heating structures were manufactured, characterised and the knowledge was refined for product development using a data-driven design approach. This includes the experimental determination of the optimal contacting variant for the used material (PLA/GNP) and the temperature-dependent resistivity from ambient temperature to 60°C. Furthermore, it was confirmed that the heat distribution is mainly dependent on the raster angle and the applied voltage.

The developed data-driven exploration approach enables a fast screening of design spaces. Thereby, robust process parameters (dependent on noise-level of input data and model uncertainty) can be predicted to extract design solutions that result in a desired heat distribution of the panel's surface. To evaluate of a current design solution, a classifier was trained to separate infeasible parameter sets (inhomogeneous temperature distribution) and to return an image of the probable heat distribution.

Further research will be performed in fields of material development and a deeper data foundation, e.g. for process parameters as well as geometry. This provides a more sophisticated model for the design process of AM heating structures. The use of matrix polymers with higher heat deflection temperatures can unlock application fields with higher continuous operating temperatures. Furthermore, the resistivity can be lowered by modifying the conductive additives and results in the scalability for large-area applications. So far, the data-driven approach is limited to simple geometries but can be further trained with data sets of more complex shapes, so that the solution space of the operating principle of AM heating structure is increased for product development. In this context, 3D-shape descriptors will be evaluated to efficiently abstract unique geometrical attributes of complex shapes and to link them with resulting heat distributions dependent on process parameters and applied voltage. This classification approach can also offer great potential in terms of a design checker by supplementing shape segmentation algorithms. For example, based on the current design of a surface, regions can be identified in which there is a disturbance of the temperature field. In addition, the collection of further data is aimed at, for example, to implement a model that defines an infill orientation as a function of location.

Acknowledgement

Funded by the German Research Foundation (DFG) – Methodical approach for additively manufactured heat-generating structures (452679573), Universal design for adaptive handles for adjustment to specific operating scenarios (452009430) and Model-based mechanical design and process planning for incremental manufacturing of multi-material workpieces (412330610). The funding sources had no influence on study design; the collection, analysis and interpretation of data; the writing of the report; or the decision to submit this article for publication.

References

An, D., Kim, N.H. and Choi, J.-H. (2015), "Practical options for selecting data-driven or physics-based prognostics algorithms with reviews", Reliability Engineering & System Safety, Vol. 133, pp. 223–236. https://doi.org/10.1016/j.ress.2014.09.014.

Bessa, M.A., Glowacki, P. and Houlder, M. (2019), "Bayesian Machine Learning in Metamaterial Design: Fragile Becomes Supercompressible", Advanced materials (Deerfield Beach, Fla.), Vol. 31 No. 48, e1904845. https://doi.org/10.1002/adma.201904845.

https://doi.org/10.1017/pds.2022.141 Published online by Cambridge University Press

Dul, S., Fambri, L. and Pegoretti, A. (2018), “Filaments Production and Fused Deposition Modelling of ABS/Carbon Nanotubes Composites”, *Nanomaterials*, Vol. 8 No. 1. https://doi.org/10.3390/nano8010049

Dul, S., Pegoretti, A. and Fambri, L. (2018), “Effects of the Nanofillers on Physical Properties of Acrylonitrile-Butadiene-Styrene Nanocomposites: Comparison of Graphene Nanoplatelets andMultiwall Carbon Nanotubes”, Nanomaterials, Vol. 8(9). https://doi.org/10.3390/nano8090674

Graphene Laboratories (2020), Inc., Black Magic 3D Conductive Graphene PLA Filament. Available at: https://www.blackmagic3d.com/Conductive-p/grphn-pla.htm (accessed 30.11.2020).

Hampel, B., Monshausen, S. and Schilling, M. (2017), “Properties and applications of electrically conductive thermoplastics for additive manufacturing of sensors”, *tm – Technisches Messen*, Vol. 84 No. 95, pp. 593-599. https://doi.org/10.1016/j.destud.2013.03.002

Hilbig, K., Watschke, H. and Vietor, T. (2020), “Technologies for economic and functional lightweight design - Design of additively manufactured heat-generating structures”, Springer, Berlin Heidelberg, pp. 142-155. https://doi.org/10.1007/978-3-662-62924-6_12

Jiang, J., Hu, G., Li, X., Xu, X., Zheng, P., et al. (2019), “Analysis and prediction of printable bridge length in fused deposition modelling based on back propagation neural network”, Virtual and Physical Prototyping, Vol. 14 No. 3, pp. 253–266. https://doi.org/10.1080/17452759.2019.1576010.

Kim, H. and Lee, S. (2020), “Characterization of Electrical Heating of Graphene/PLA Honeycomb Structure Composite Manufactured by CFDM 3D Printer”, *Fashion and Textiles*, Vol. 7 No. 8, pp. 1-18. https://doi.org/10.1186/s40691-020-0204-2

Leigh, S.J., Bradley, R.J., Purssel, C.P., Billson, D.R. and Hutchins, D.A. (2012), “Integration of physically-based and data-driven approaches for thermal field prediction in additive manufacturing”, PLoS One, Vol. 11. https://doi.org/10.1371/journal.pone.0049365

Li-Hua, S, Zhao, B., Zhang, Q., Xing, Y., and Zhang, K. (2020), “A Simple, Low-Cost Conductive Composite Material for 3D Printing of Electronic Sensors”, *Extreme Mechanics Letters*, Vol. 39. https://doi.org/10.1016/j.eml.2020.100793

Rahmah, N. and Sitanggang, I.S. (2016), “Determination of Optimal Epsilon (Eps) Value on DBSCAN Algorithm to Clustering Data on Peatland Hotspots in Sumatra”, IOP Conference Series: Earth and Environmental Science, Vol. 31, p. 12012. https://doi.org/10.1088/1755-1315/31/1/012012.

Reuter, M., Wolter, F.-E. and Peinecke, N. (2006), “Laplace–Beltrami spectra as ‘Shape-DNA’ of surfaces and solids”, Computer-Aided Design, Vol. 38 No. 4, pp. 342–366. https://doi.org/10.1016/j.cad.2005.10.011.

Roy, M. and Wodo, O. (2020), “Data-driven modeling of thermal history in additive manufacturing”, Additive Manufacturing, Vol. 32, p. 101017. https://doi.org/10.1016/j.addma.2019.101017.

Simonyan, K. and Zisserman, A. (2014), "Very Deep Convolutional Networks for Large-Scale Image Recognition", (2015), Proceedings of the 2015 IEEE 9th International Conference on Semantic Computing (IEEE ICSC 2015). https://arxiv.org/abs/1409.1556

Tirado-Garcia, I, Garcia-Gonzalez, D., Garzon-Hernandez, S., Rusinek, A.,Robles, G., Martinez-Tarifa, J.M. and Arias, A. (2021), “Conductive 3D printed PLA composites: On the interplay of mechanical,electrical and thermal behaviours”, *Composite Structures*, Vol. 265. https://doi.org/10.1016/j.compstruct.2021.113744

Watschke, H. (2019), "Methodisches Konstruieren für Multi-Material-Bauweisen hergestellt mittels Materialextrusion", [PhD Thesis], Technische Universität Braunschweig. https://doi.org/10.24355/dbbs.084-202004201049-0

Watschke, H., Hilbig, K. and Vietor, T. (2019), “Design and Characterization of Electrically Conductive Structures Additively Manufactured by Material Extrusion”, *Applied Sciences*, Vol. 9 No. 4. https://doi.org/10.3390/app9040779

Wang, Y., Blache, R., Zheng, P. and Xu, X. (2018), “A Knowledge Management System to Support Design for Additive Manufacturing Using Bayesian Networks”, Journal of Mechanical Design, Vol. 140 No. 5. https://doi.org/10.1115/1.4039201.

Xiong, Y., Duong, P.L.T., Wang, D., Park, S.-I., Ge, Q., et al. (2019), “Data-Driven Design Space Exploration and Exploitation for Design for Additive Manufacturing”, Journal of Mechanical Design, Vol. 141 No. 10. https://doi.org/10.1115/1.4043587.

Yin, S., Ding, S.X., Xie, X. and Luo, H. (2014), “A Review on Basic Data-Driven Approaches for Industrial Process Monitoring”, IEEE Transactions on Industrial Electronics, Vol. 61 No. 11, pp. 6418–6428. https://doi.org/10.1109/TIE.2014.2301773.

Zhang, Y. and Moon, S.K. (2021), “Data-driven design strategy in fused filament fabrication: status and opportunities”, Journal of Computational Design and Engineering, Vol. 8 No. 2, pp. 489–509. https://doi.org/10.1093/jcde/qwaa094.

Zhuang, Y., Song, W., Ning, G., Sun, X., Sun, Z., Xu, Z., Zhang, B., Chen, Y. and Tao, S. (2017), “3D–printing of materials with anisotropic heat distribution using conductive polylactic acid composites”, *Materials & Design*, Vol. 126, pp. 135-140. https://doi.org/10.1016/j.matdes.2017.04.047.